Universal device for two-qubit entangled measurements via photonic quantum walks

Wen-Zhe Yan,[1,2,3] Zhibo Hou,[1,2,3,*] Jun-Feng Tang,[1,2,3] Guo-Yong Xiang,[1,2,3,†] Chuan-Feng Li,[1,2,3] Guang-Can Guo,[1,2,3] and Marc-Olivier Renou[4,5,6,‡]

[1] *CAS Key Laboratory of Quantum Information, University of Science and Technology of China, Hefei, 230026, People's Republic of China*

[2] *CAS Center For Excellence in Quantum Information and Quantum Physics, University of Science and Technology of China, Hefei, 230026, People's Republic of China*

[3] *Hefei National Laboratory, University of Science and Technology of China, Hefei 230088, People's Republic of China*

[4] *ICFO—Institut de Ciencies Fotoniques, Barcelona Institute of Science and Technology, Castelldefels, Barcelona, Spain*

[5] *Inria Saclay, Bâtiment Alan Turing, 1 Rue Honoré d'Estienne d'Orves, 91120 Palaiseau, France*

[6] *Centre de Physique Théorique, Ecole Polytechnique, Institut Polytechnique de Paris, Route de Saclay, 91128 Palaiseau, France*

(Received 21 June 2023; accepted 11 September 2023; published 12 October 2023)

Sophisticated positive-operator-valued measures (POVMs) are fundamental to obtain a quantum advantage in many informational problems but are difficult to implement. We design a universal measurement device composed of cascaded quantum-walk modules able to realize arbitrary entangled POVMs on two qubits. Only parameters in the modules need reprogramming for different POVMs. We apply our device to the task of direction guessing, realizing nine different five-outcome entangled measurements (fidelities above 0.9850) via nine-step photonic quantum walks, recovering optimal direction guessing from nonideal input states. Our work marks an important step toward building a universal versatile quantum measurement device able to implement optimal measurements for various quantum information tasks.

DOI: 10.1103/PhysRevApplied.20.044032

I. INTRODUCTION

The manipulation of quantum information outperforms the manipulation of classical information for many informational problems [1–8]. Being able to implement powerful quantum measurements to extract information is fundamental to obtain such a quantum advantage [9–13]. This requires the ability to realize nonprojective entangled positive-operator-valued measures (POVMs). On one hand, entangled (or joint) quantum measurements are represented by measurement operators containing at least one entangled eigenstate [5]. A prominent example is collective measurements on identically prepared quantum systems [14,15], which view the ensemble as a whole and manipulate entanglement between the copies during the measuring process. Entangled measurements offer advantages over separable measurements in information extraction [14–16]. It is entanglement in the measurements rather than in the states that provides the advantage. Entangled measurements enhance the estimation of quantum states [9,12,15,16] and lead to higher precision in quantum metrology [17,18]. They have also found applications in numerous tasks such as entanglement purification [19], overlap estimation [20] and quantum change point detection [21]. Moreover, they can be used to suppress measurement backaction in quantum thermodynamics [22, 23]. On the other hand, POVMs [2] are the most-general description of quantum measurements. A POVM is a set of positive but not necessarily orthogonal operators summing up to the identity. In many scenarios, nonprojective POVMs are more powerful than projective measurements owing to their diverse forms and capabilities [12,14,22,24–28]. A paradigmatic example is a skill called "abstention," where the measurements include an inconclusive outcome as in unambiguous discrimination [29,30] and probabilistic quantum metrology [27]. This is relevant in a context where postselection is allowed, or if a noncooperative agent is using apparent losses to increase its estimation score. If a POVM contains entangled operators, it is an entangled POVM. Experimental realization of the powerful entangled POVMs is of paramount importance in practical quantum tasks.

*houzhibo@ustc.edu.cn
†gyxiang@ustc.edu.cn
‡marc-olivier.renou@icfo.eu

However, how to implement arbitrary entangled POVMs is still an experimental challenge. What is more challenging but desirable is to realize all entangled measurements with one universal measurement device. So far, even for simple two-qubit cases, there exist only some special entangled measurement devices [23,31–33], whose versatility is limited. In particular, there is a recent experimental advance [34] that implements arbitrary two-qubit projective entangled measurements on superconducting and trapped-ion systems. Nevertheless, an experimentally amenable method to realize arbitrary nonprojective entangled measurements is still lacking.

In this work, we develop a general recipe for implementing arbitrary two-qubit entangled POVMs using quantum walks [35]. We use cascaded quantum-walk modules with programmable coin operators to construct a universal measurement device. Our measurement device is universal in the way that we just reprogram the parameters (waveplate rotation angles) to realize different entangled measurements. As an experimental application, we focus on the fundamental problem of direction estimation [15,16,28,36–40]. We consider the probabilistic protocol where abstention is used to increase the measurement accuracy. Here, the optimal measurement is described by a five-output entangled two-qubit POVM including an abstention operator, and varies with the code state, so it cannot be performed on previous special measurement devices. Our universal design makes it possible to implement different optimal measurements on a single device containing a nine-step photonic quantum walk, experimentally recovering the maximal guessing score even with states which are suboptimal in the standard deterministic protocol [16,33,36]. Note that our design uses two degrees of freedom (DOF) of a single photon to encode two qubits [41–44]. However, it can be extended to collective measurements on two photons by applying the technique of quantum joining [45] at the beginning, where the polarization state of two input photons is transferred into a quantum state of a single output photon in the Hilbert space of its polarization and path DOF.

II. REALIZING ARBITRARY TWO-QUBIT ENTANGLED POVMS VIA QUANTUM WALKS

Quantum walks are a powerful tool for implementing general POVMs [35,46]. A one-dimensional discrete-time quantum walk is a process in which the evolution of a quantum particle (walker) on a lattice depends on the state of a two-level system (coin). The joint system is characterized by two DOF labeled as $|x, c\rangle$, where $x = \ldots, -1, 0, 1, \ldots$ denotes the walker position and $c = 0, 1$ denotes the coin state. The dynamics correspond to several unitary steps. At step t, the unitary operator is given by $U(t) = TC(t)$, where $C(t) = \sum_x |x\rangle\langle x| \otimes C(x, t)$ is determined by site-dependent coin operators $C(x, t)$ representing coin toss and

$$T = \sum_x |x + 1, 0\rangle\langle x, 0| + |x - 1, 1\rangle\langle x, 1| \qquad (1)$$

is the conditional translation operator, updating the walker position on the basis of the coin state. After n steps, the evolution is given by $U = \prod_{t=1}^{n} TC(t)$.

It is proven that any POVM on a single qubit, concretely the coin qubit, can be realized by measuring the walker position after certain steps by choosing the coin operators properly [35]. This has been implemented experimentally [47,48]. However, for two-qubit systems, the general method is still lacking.

Here we devise an experimental recipe for implementing arbitrary two-qubit entangled POVMs via quantum walks, as illustrated in Fig. 1. We take the two-level coin qubit and the walker in positions 1 and -1 as the two-qubit system of interest, while other positions of the walker act as ancillary levels. Consider a rank-1 POVM $\{E_1, E_2, \ldots, E_n\}$,where $E_i = a_i|\psi_i\rangle\langle\psi_i|$, $|\psi_i\rangle$ are normalized two-qubit states and $0 < a_i \leq 1$. Each element E_i is implemented by a four-step quantum-walk module. The fixed coin operators NOT and $\mathbb{1}$ refer to the NOT gate and the identity operator. We adapt the method in Ref. [46] to find the algorithm for calculating

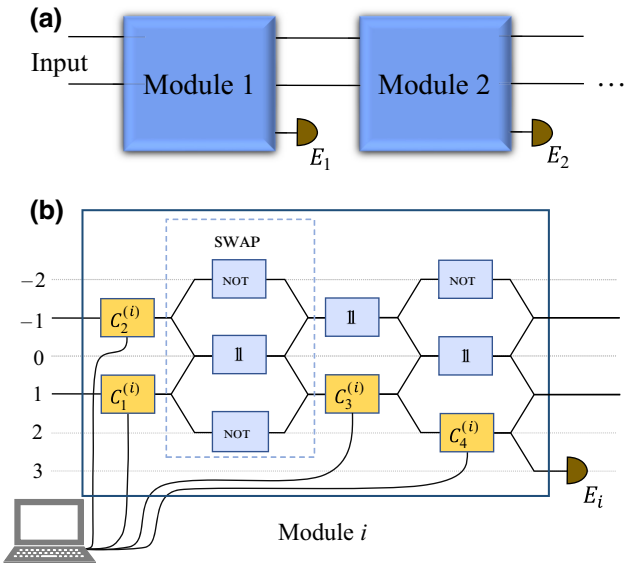

FIG. 1. General method for implementing an arbitrary two-qubit entangled POVM via cascaded quantum-walk modules. The coin qubit and the walker in positions 1 and -1 are taken as the two-qubit system of interest. (a) Each POVM element E_i is implemented by a quantum-walk module iteratively. (b) Each module contains a four-step quantum walk. Positions 3, 2, 0, and -2 act as ancillary levels. Coin operators $C_j^{(i)} (j = 1, \ldots, 4)$ are programmable and are determined by the target POVM.

the programmable coin operators $C_j^{(i)}(j = 1, \ldots, 4)$ in the ith module, which is elaborated as follows.

Let $C_4^{(i)}$ be a real matrix in the form of

$$C_4^{(i)} = \begin{pmatrix} \alpha_i & \beta_i \\ \beta_i & -\alpha_i \end{pmatrix}, \tag{2}$$

where α_i and β_i are parameters to be determined.

Suppose $|\varphi\rangle$ is the two-qubit input state to be measured. Let $|1,0\rangle = |1\rangle$, $|1,1\rangle = |2\rangle$, $|-1,0\rangle = |3\rangle$, and $|-1,1\rangle = |4\rangle$. Introduce a matrix K_i, which is defined by the relation that the component of the input state entering the ith module reads $K_i|\varphi\rangle$. Thus, $K_1 = \mathbb{1}$ and

$$K_{i+1} = \begin{pmatrix} 0 & 0 & 1 & 0 \\ \beta_i & 0 & 0 & 0 \\ 0 & 0 & 0 & 1 \\ 0 & 1 & 0 & 0 \end{pmatrix} \begin{pmatrix} C_3^{(i)} & 0 \\ 0 & \mathbb{1} \end{pmatrix} \begin{pmatrix} 0 & 0 & 1 & 0 \\ 1 & 0 & 0 & 0 \\ 0 & 0 & 0 & 1 \\ 0 & 1 & 0 & 0 \end{pmatrix} \begin{pmatrix} C_1^{(i)} & 0 \\ 0 & C_2^{(i)} \end{pmatrix} K_i. \tag{3}$$

Introduce a normalized ket $|\eta_i\rangle = b_i^{-1} K_i^{\dagger+} |\psi_i\rangle$, where $b_i := \|K_i^{\dagger+}|\psi_i\rangle\|$ and $K_i^{\dagger+}$ is the Moore-Penrose generalized inverse of $K_i^{\dagger}$. Then we can determine all the coin operators $C_j^{(i)}$ recursively. The coin operators $C_1^{(i)}$, $C_2^{(i)}$, and $C_3^{(i)}$ are chosen such that

$$\begin{pmatrix} C_3^{(i)} & 0 \\ 0 & \mathbb{1} \end{pmatrix} \begin{pmatrix} 0 & 0 & 1 & 0 \\ 1 & 0 & 0 & 0 \\ 0 & 0 & 0 & 1 \\ 0 & 1 & 0 & 0 \end{pmatrix} \begin{pmatrix} C_1^{(i)} & 0 \\ 0 & C_2^{(i)} \end{pmatrix} |\eta_i\rangle = |1\rangle, \tag{4}$$

implying that after the third step of the ith module, the amplitude entering position 2 is $b_i^{-1}\langle\psi_i|K_i^+ K_i|\varphi\rangle$. The parameters α_i and β_i are given by

$$\alpha_i = b_i\sqrt{a_i}, \quad \beta_i = \sqrt{1 - b_i^2 a_i}. \tag{5}$$

Therefore, after the fourth step, the probability of finding the walker at detector "E_i" reads

$$\begin{aligned} p_i &= \left|\sqrt{a_i}\langle\psi_i|K_i^+ K_i|\varphi\rangle\right|^2 = \left|\sqrt{a_i}\langle\psi_i|P_{K_i}|\varphi\rangle\right|^2 \\ &= a_i\left|\langle\psi_i|\varphi\rangle\right|^2 = \mathrm{Tr}\left(E_i|\varphi\rangle\langle\varphi|\right), \end{aligned} \tag{6}$$

demonstrating that the desired POVM is realized. Here P_{K_i} is the projector onto $\mathrm{supp}(K_i)$. The third equality follows from the fact that $|\psi_i\rangle \in \mathrm{supp}(K_i)$, which can be obtained from the inequality

$$E_i = a_i|\psi_i\rangle\langle\psi_i| \le \mathbb{1} - \sum_{l=1}^{i-1} E_l = K_i^{\dagger} K_i. \tag{7}$$

Additionally, this inequality also implies that

$$\alpha_i^2 = a_i b_i^2 = a_i\|K_i^{\dagger+}|\psi_i\rangle\langle\psi_i|K_i^+\| \le 1; \tag{8}$$

thus, $C_4^{(i)}$ is well defined. For the last element E_n, we just sum the probabilities of finding the walker in positions 1 and -1 at the exit of the $(n-1)$th module.

It is worth noting that we design a "SWAP" structure that implements a unitary operator

$$\mathrm{U} = \begin{pmatrix} 0 & 0 & 1 & 0 \\ 1 & 0 & 0 & 0 \\ 0 & 0 & 0 & 1 \\ 0 & 1 & 0 & 0 \end{pmatrix} = (\mathbb{1} \otimes \mathrm{NOT})\mathrm{SWAP}, \tag{9}$$

which makes the originally difficult walker operation easy by swapping the walker qubit for the operation-friendly coin qubit. Additionally, under some specific conditions, the construction in Fig. 1 can be further simplified.

A universal measurement device with reprogramming can realize a series of measurements without the setup needing to be rebuilt. As we show in the task of direction guessing assisted by abstention, to recover the maximal guessing score for different code states, different entangled POVMs are required, which is difficult to realize with previous special measurement devices tailored to a single measurement.

III. OPTIMAL DIRECTION GUESSING ASSISTED BY ABSTENTION

As an application, we consider the task of optimal direction guessing assisted by abstention. Concretely, Alice is given a rotated two-spin-1/2 state $|\Psi_{\mathbf{n}}\rangle := U_{\mathbf{n}}|\Psi_{\mathbf{z}}\rangle$, where $|\Psi_{\mathbf{z}}\rangle$ is the initial state, $U_{\mathbf{n}}$ is the unitary representation of a rotation mapping states of direction $+\mathbf{z}$ into states of direction $\mathbf{n}$, and $\mathbf{n}$ is selected uniformly at random. She measures it to guess its direction and is allowed to not answer with probability $Q = 1 - \bar{Q}$. The measurement is characterized by POVM $\Pi = \{\Pi_{\hat{\mathbf{n}}}\} \cup \{\Pi_{\mathrm{abst}}\}$, where $\Pi_{\hat{\mathbf{n}}}$ generates a guess $\hat{\mathbf{n}}$ and Π_{abst} corresponds to abstention. The abstention operator Π_{abst} is taken to be rotation invariant, i.e., $\Pi_{\mathrm{abst}} = \lambda_0 \mathbb{1}_{\mathcal{H}_0} + \lambda_1 \mathbb{1}_{\mathcal{H}_1}$ [27,28], where $\mathcal{H}_0$ is the singlet space spanned by $|\psi^-\rangle$, $\mathcal{H}_1$ is the triplet space spanned by $|\psi^+\rangle, |\phi^\pm\rangle$, in which $|\phi^\pm\rangle = 1/\sqrt{2}(|00\rangle \pm |11\rangle)$, $|\psi^\pm\rangle = 1/\sqrt{2}(|01\rangle \pm |10\rangle)$, and $\lambda_0, \lambda_1 \in [0,1]$ can be optimized to obtain the best guess. We measure Alice's performances with two scores $s \in \{f, \delta\}$. The first is the fidelity score $f(\mathbf{n}, \hat{\mathbf{n}}) = 1/2(1 + \mathbf{n}\cdot\hat{\mathbf{n}})$. The second is the

maximum likelihood score characterized by a Dirac distribution $\delta(\mathbf{n},\hat{\mathbf{n}})$ [49], which measures only the likelihood to perform a perfect guess. The average guessing score is computed only for the cases in which she answers, given by

$$s_{\text{av}} = \frac{1}{1-Q}\int d\mathbf{n}d\hat{\mathbf{n}}s(\mathbf{n},\hat{\mathbf{n}})\text{Tr}\left(\Pi_{\hat{\mathbf{n}}}\Psi_{\mathbf{n}}\right), \tag{10}$$

where $\Psi_{\mathbf{n}} = |\Psi_{\mathbf{n}}\rangle\langle\Psi_{\mathbf{n}}|$ and $Q = \int d\mathbf{n}\text{Tr}\left(\Pi_{\text{abst}}\Psi_{\mathbf{n}}\right)$. We write a general initial state as

$$|\Psi_z\rangle = c_0|\psi^-\rangle + c_1|\psi^{\text{sym}}\rangle, \tag{11}$$

where $|\psi^{\text{sym}}\rangle \in \mathcal{H}_1$.

It can be proven that in the standard deterministic protocols where abstention is not allowed, i.e., $\lambda_0 = \lambda_1 = 0$, the optimal fidelity $f_{\max} = (3+\sqrt{3})/6$ is obtained only for $c_0 = c_1 = 1/\sqrt{2}, |\psi^{\text{sym}}\rangle = |\psi^+\rangle$ and the optimal maximum likelihood score $\delta_{\max} = 4$ is obtained only for $c_0 = 1/2$ and $c_1 = \sqrt{3}/2$ independently of $|\psi^{\text{sym}}\rangle \in \mathcal{H}_1$. By contrast, in our probabilistic protocol, which succeeds with probability $\bar{Q}$, abstention acts as a filter to discard unfavorable outcomes and makes it possible to recover the optimal guessing score even from suboptimal states (see Appendix A). Concretely, Alice can always reach $f_{\max}$ under the condition that $c_0, c_1 \neq 0, |\psi^{\text{sym}}\rangle = |\psi^+\rangle$ and that she is allowed to not answer with probability $Q \geq 1 - 2\min(c_0^2, c_1^2)$, by taking $\bar{\lambda}_k = 1 - \lambda_k = \bar{Q}/2c_k^2$. She can also reach $\delta_{\max}$ under the condition that $c_0, c_1 \neq 0$ and that she is allowed to not answer with probability $Q \geq 1 - 4\min(c_0^2, c_1^2/3)$, by taking $\bar{\lambda}_0 = \bar{Q}/4c_0^2$ and $\bar{\lambda}_1 = 3\bar{Q}/4c_1^2$. The condition $c_0, c_1 \neq 0$ is intuitive because the code states should explore the full Hilbert space $\mathcal{H} = \mathcal{H}_0 \oplus \mathcal{H}_1$ to obtain a good encoding property [16]. In both cases, Alice simulates the behavior of an optimal initial state using abstention.

We now assume that $|\psi^{\text{sym}}\rangle = |\psi^+\rangle$. The optimal POVM elements (in addition to Π_{abst}) can be taken to be four rank-1 operators $\Pi_{\hat{\mathbf{n}}_i} = |\Phi_{\hat{\mathbf{n}}_i}\rangle\langle\Phi_{\hat{\mathbf{n}}_i}|$, where

$$|\Phi_{\hat{\mathbf{n}}_i}\rangle = \frac{\sqrt{\bar{\lambda}_0}}{2}|\psi^-_{\hat{\mathbf{n}}_i}\rangle + \frac{\sqrt{3\bar{\lambda}_1}}{2}|\psi^+_{\hat{\mathbf{n}}_i}\rangle, \quad i = 1,2,3,4, \tag{12}$$

are subnormalized vectors and $\hat{\mathbf{n}}_i$ points at the four extremities of a tetrahedron. With use of the method in Fig. 1, the above two-qubit entangled POVM with any $\bar{\lambda}_0, \bar{\lambda}_1 \in [0,1]$ can be implemented on a single device containing four cascaded quantum-walk modules (16-step quantum walks). Under the restriction $\bar{\lambda}_1 = 1$, i.e., abstention is applied only in $\mathcal{H}_0$, the construction can be simplified to a nine-step quantum walk for experimental ease (see Appendix B).

IV. EXPERIMENTAL SETUP

We experimentally build the measurement device to implement the entangled POVM of Eq. (12) and demonstrate the optimal direction guessing with abstention (see

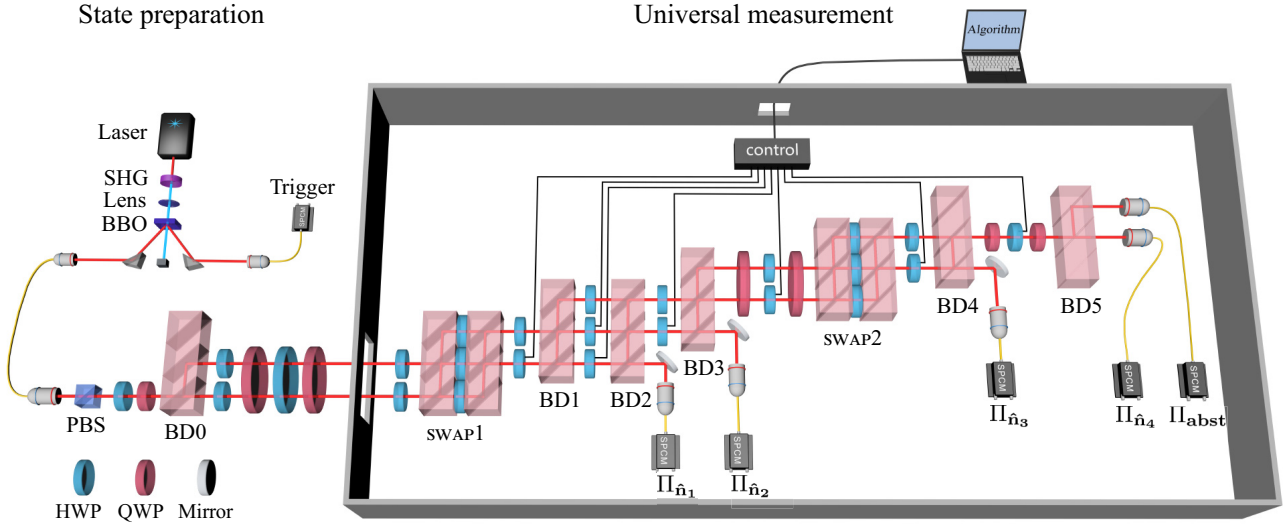

FIG. 2. Experimental setup for implementing two-qubit entangled measurements and its application in abstention-assisted direction guessing. In the state-preparation module, the direction to be estimated is encoded into a two-qubit state in the path and polarization degrees of freedom. Then the universal measurement device performs the optimal POVM via a nine-step quantum walk. The coin operators are realized by a sequence of HWPs and QWPs, whose rotation angles are controlled and programmed to implement different measurements. The conditional translation operator T is realized by BDs, each of which includes three PBS coatings separated by 2 mm. The "SWAP" structure contains a compact two-step-quantum-walk architecture, which is composed of three HWPs and two BDs. The five single-photon detectors correspond to the five POVM elements. BBO, β-barium borate; SHG, second-harmonic generation.

TABLE I. Overall fidelities of the implemented POVMs. $\bar{\lambda}_1 = 1$ is fixed and $\bar{\lambda}_0$ is determined by c_0 according to the optimization conditions. Each data point is the average over 25 repetitions of 20 000 runs. The error bars indicate the standard deviation of 25 repetitions.

Likelihood score	c_0	0.5	0.6	0.7	0.8	0.9
	$\bar{\lambda}_0$	1	0.5926	0.3469	0.1875	0.0782
	Overall fidelity	0.9854(1)	0.9857(5)	0.9852(7)	0.9893(7)	0.9850(7)
Fidelity score	c_0	0.7071	0.7571	0.8071	0.8571	0.9071
	$\bar{\lambda}_0$	1	0.7446	0.5351	0.3612	0.2153
	Overall fidelity	0.9854(1)	0.9876(9)	0.9866(8)	0.9856(7)	0.9870(6)

Fig. 2). We fix $\bar{\lambda}_1 = 1$ and optimize $\bar{\lambda}_0$ to recover the maximum score. The polarization and path DOF of a single photon act as the coin and the walker, respectively. The site-dependent coin operators are realized by a sequence of half-wave plates (HWPs) and quarter-wave plates (QWPs). The conditional translation operator is realized by interferometrically stable beam displacers (BDs), which displace the component with horizontal polarization away from the component with vertical polarization. In our experimental setup, we use a structure composed of three bonded polarizing beam splitters (PBSs) as a BD.

The direction $\mathbf{n}$ is encoded into a two-qubit state in the path and polarization DOF through a state-preparation process (see Appendix C). Next, the universal measurement device performs the optimal POVMs via a nine-step photonic quantum walk. We reprogram the rotation angles of some wave plates to implement different measurements (see specific angles in Appendix D). To reduce the phase instability of the interferometers, which is the main problem leading to the decrease of precision as the number of steps of walks increases, we concatenate two BDs and three HWPs respectively set at 45°, 0°, and 45° as a compact "SWAP" structure. This compactness makes the structure more robust with regard to environmental perturbations. The five single-photon-counting modules at the end correspond to the five POVM elements. On the basis of the measurement outcome, Alice gives her answer $\hat{\mathbf{n}}$ or abstains.

V. EXPERIMENTAL RESULTS

Because we fix $\bar{\lambda}_1 = 1$ and optimize $\bar{\lambda}_0$, The maximum likelihood (fidelity) score can be recovered for $1/2 \le c_0 < 1$ ($1/\sqrt{2} \le c_0 < 1$). We choose five points of c_0 in each situation (see Table I), corresponding to a total of nine measurements.

We first perform quantum measurement tomography to accurately characterize the measurements that were actually realized. We prepare and send 20 input states (the mutually unbiased bases for two qubits) to the measurement device. We reconstruct the measurements with the method in Ref. [50], obtaining overall fidelities above 0.985 for the implemented POVMs, demonstrating a high-quality realization (see Table I).

Next we implement the optimal direction guessing scheme. The experimental results are illustrated in Fig. 3 (red circles). The scores we obtain coincide well with theoretical predictions (solid red line). Note that the deviation between the experimental score and the ideal score tends to increase with increase of c_0, due to the term $1/(1-Q)$ in Eq. (10), which increases with c_0 (see Appendix E). We also plot the theoretical scores in the no-abstention case (solid blue line). Hence, for the maximum likelihood score, our experiments almost achieved the maximum $\delta_{\max} = 4$ for suboptimal states using abstention, which without abstention would be possible for $c_0 = 1/2$ only. The abstention advantage increases with the distance between the suboptimal states and the optimal state. Specifically, for the suboptimal state corresponding to $c_0 = 0.9$, we obtain an experimental score of 3.9162, to be compared with the theoretical value of 2.7390 without abstention:

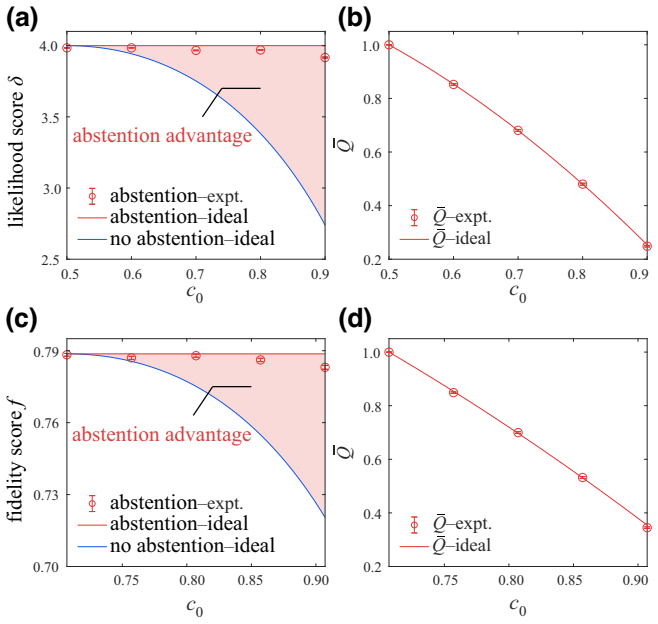

FIG. 3. Experimental results for the optimal direction guessing. For (a) the likelihood score and (c) the fidelity score, it is experimentally proved that the suboptimal states can also achieve the maximum score with abstention. The corresponding acceptance rate $\bar{Q}$ in each case is shown in (b),(d) respectively.

we reduce the deviation from $\delta_{\max}$ by a factor of about 15. Similarly, for the fidelity score, we almost recover the maximum $f_{\max} = (3+\sqrt{3})/6 \approx 0.7887$ for suboptimal states using abstention. For the suboptimal state corresponding to $c_0 = 0.9071$, we obtain an experimental score of 0.7831, to be compared with the theoretical value of 0.7204 without abstention: we reduce the deviation from $f_{\max}$ by a factor of about 12. The corresponding acceptance rates $\bar{Q}$ are shown in Figs. 3(b) and 3(d).

VI. SUMMARY

We proposed a universal method for realizing arbitrary two-qubit POVMs using quantum walks. We experimentally implemented nine optimal measurements in the direction-guessing task on a single device with high fidelities, demonstrating the malleability of our method for concretely implementing complex many-output POVMs.

The application is focused on optimal orienting with a two-qubit input state. Here, a nonzero component of the state in the singlet space allows better encoding of the direction in the full Hilbert space. An effect is theoretically predicted for three-qubit input states. In that case, the Hilbert space decomposes into a spin 1/2 with multiplicity 2 and a spin 3/2. One can, in principle, exploit the multiplicity of the spin 1/2 to perform a dense coding encryption of the rotation in the input state, which results in better direction-guessing scores [39,40]. Being able to witness this nonintuitive effect (it was overlooked in the literature [40]; see, e.g., Refs. [36–38]) is an interesting experimental challenge, which would require manipulation and measurement of three-qubit states. By use of more paths for the walker or use two-dimensional quantum walks, our method can be further extended to realize entangled POVMs on multiqubit states. Integrated optics [51] is a potential platform for more-sophisticated many-path quantum walks.

ACKNOWLEDGMENTS

We thank Nicolas Gisin, Antonio Acín, and Enky Oudot for valuable discussions. The work at the University of Science and Technology of China is supported by the National Natural Science Foundation of China (Grants No. 12134014, No. 61905234, No. 11974335, and No. 11774334), the Key Research Program of Frontier Sciences, Chinese Academy of Sciences (Grant No. QYZDYSSW-SLH003), the Innovation Program for Quantum Science and Technology (Grant No. 2021ZD0301203), University of Science and Technology of China Research Funds of the Double First-Class Initiative (Grant No. YD2030002007), and the Fundamental Research Funds for the Central Universities (Grant No. WK2470000035). M.-O.R. is supported by Grant No. PCI2021-122022-2B financed by MCIN/AEI/10.13039/501100011033 and by the European Union NextGenerationEU Recovery and Resilience Facility and the Swiss National Fund Early Mobility Grants (Grant No. P2GEP2_19144/2), and acknowledges the Government of Spain [FIS2020-TRANQI and Severo Ochoa CEX2019-000910-S (MCIN/AEI/10.13039/50110 0011033)], Fundació Cellex, Fundació Mir-Puig, Generalitat de Catalunya (CERCA, AGAUR SGR 1381), and the European Research Council Advanced Grant CERQUTE.

APPENDIX A: OPTIMAL STATES AND MEASUREMENTS IN DIRECTION GUESSING TASKS

In this appendix, we provide details for computing the maximum score and the optimal states and measurements in the direction-guessing tasks mentioned in Sec. III.

1. Standard deterministic direction guessing

The rotation operator can be written as $U_{\mathbf{n}} = u_{\mathbf{n}} \otimes u_{\mathbf{n}}$, where $u_{\mathbf{n}} \in \mathrm{SU}(2)$ takes the direction $+\mathbf{z}$ into $\mathbf{n}$. The guessing score $s \in \{f, \delta\}$ is group invariant, i.e., $s(\mathbf{n}, \hat{\mathbf{n}}) = s(u_{\mathbf{n}}, u_{\hat{\mathbf{n}}}) = s(u_{\hat{\mathbf{n}}}^{-1} u_{\mathbf{n}}, \mathbb{1}) \equiv s(u_{\hat{\mathbf{n}}}^{-1} u_{\mathbf{n}})$. One can restrict Alice's POVM measurement to be covariant, i.e., $\Pi_{\hat{\mathbf{n}}} = U_{\hat{\mathbf{n}}} \Pi_z U_{\hat{\mathbf{n}}}^{\dagger}$ [52]. The mean score is given by

$$\begin{aligned} s_{\mathrm{av}} &= \int d\mathbf{n} d\hat{\mathbf{n}} s(\mathbf{n}, \hat{\mathbf{n}}) \mathrm{Tr}\left(\Pi_{\hat{\mathbf{n}}} \Psi_{\mathbf{n}}\right) \\ &= \int d\mathbf{n} d\hat{\mathbf{n}} s(u_{\hat{\mathbf{n}}}^{-1} u_{\mathbf{n}}) \mathrm{Tr}\left(U_{\hat{\mathbf{n}}} \Pi_z U_{\hat{\mathbf{n}}}^{\dagger} \cdot U_{\mathbf{n}} \Psi_z U_{\mathbf{n}}^{\dagger}\right) \\ &= \int d\mathbf{n} s(\mathbf{n}, +\mathbf{z}) \mathrm{Tr}\left(\Pi_z U_{\mathbf{n}} \Psi_z U_{\mathbf{n}}^{\dagger}\right) \\ &= \mathrm{Tr}\left(\Pi_z F\right), \end{aligned} \tag{A1}$$

where $F = \int d\mathbf{n} s(\mathbf{n}, +\mathbf{z}) U_{\mathbf{n}} \Psi_z U_{\mathbf{n}}^{\dagger}$. In the third equality we perform the substitution $u_{\hat{\mathbf{n}}}^{-1} u_{\mathbf{n}} \to u_{\mathbf{n}}$.

Let $\Pi_z = |\eta\rangle\langle\eta|$. The normalization condition $\int d\hat{\mathbf{n}} U_{\hat{\mathbf{n}}} \Pi_z U_{\hat{\mathbf{n}}}^{\dagger} = \mathbb{1}$ gives

$$|\eta\rangle = |\psi^-\rangle + \sqrt{3}|\phi^{\mathrm{sym}}\rangle, \tag{A2}$$

where only $|\phi^{\mathrm{sym}}\rangle \in \mathcal{H}_1$ can be optimized. Note that as we perform integration over some probability density, $|\eta\rangle$ is un-normalized.

a. Maximum likelihood score

With the maximum likelihood score $\delta(\mathbf{n}, \hat{\mathbf{n}})$, we have

$$F_{\delta} = \int d\mathbf{n} \delta(\mathbf{n}, +\mathbf{z}) U_{\mathbf{n}} \Psi_z U_{\mathbf{n}}^{\dagger} = \Psi_z. \tag{A3}$$

For the average score $\delta_{\rm av}$, we have

$$\begin{aligned}\delta_{\rm av} &= {\rm Tr}\,(\Pi_z F_\delta) = {\rm Tr}\,(\Pi_z \Psi_z) = |\langle\eta|\Psi_z\rangle|^2 \\ &= |c_0 + \sqrt{3}c_1\langle\phi^{\rm sym}|\psi^{\rm sym}\rangle|^2. \end{aligned} \tag{A4}$$

Hence, for a given initial state $|\Psi_z\rangle$ described by Eq. (11), the corresponding optimal measurement is given by imposing $|\phi^{\rm sym}\rangle = |\psi^{\rm sym}\rangle$ in $|\eta\rangle$. Then we have

$$\delta_{\rm av} = |c_0 + \sqrt{3}c_1|^2. \tag{A5}$$

Hence, optimal states are for $c_0 = 1/2$ and $c_1 = \sqrt{3}/2$, with which we obtain the optimal maximum likelihood score

$$\delta_{\rm max} = 4. \tag{A6}$$

b. Fidelity score

For the general case $|\psi^{\rm sym}\rangle = \alpha|\phi^+\rangle + \beta|\psi^+\rangle + \gamma|\phi^-\rangle$, we have

$$\begin{aligned}F_f(\alpha,\beta,\gamma) =& \frac{|c_0|^2}{2}\mathbb{1}_{\mathcal{H}_0} + \frac{|c_1|^2}{6}\mathbb{1}_{\mathcal{H}_1} + \frac{1}{6}(c_0 c_1^* \beta^* |\psi^-\rangle\langle\psi^+| \\ &+ \frac{|c_1|^2\alpha\gamma^*}{2}(|\phi^+\rangle\langle\phi^-| + |\phi^-\rangle\langle\phi^+|) \\ &+ {\rm H.c.}). \end{aligned} \tag{A7}$$

Let $|\phi^{\rm sym}\rangle = a|\phi^+\rangle + b|\psi^+\rangle + c|\phi^-\rangle$. The average score is given by

$$\begin{aligned}f_{\rm av}(\alpha,\beta,\gamma) &= {\rm Tr}\left(\Pi_z F_f(\alpha,\beta,\gamma)\right) \\ &= \frac{1}{2} + \frac{\sqrt{3}}{6}(c_0 c_1^* \beta^* b + \sqrt{3}|c_1|^2\alpha\gamma^* {\rm Re}(a^* c) \\ &\quad + {\rm c.c.}). \end{aligned} \tag{A8}$$

To maximize $f_{\rm av}$, we can restrict ourselves to real positive coefficients (due to the triangular inequality). Then

$$\begin{aligned}f_{\rm av} &= \frac{1}{2} + \frac{\sqrt{3}}{3}(c_0 c_1 \beta b + \sqrt{3}c_1^2\alpha\gamma ac) \\ &\le \frac{1}{2} + \frac{\sqrt{3}}{3}(c_0 c_1\beta b + \frac{\sqrt{3}}{4}c_1^2(1-\beta^2)(1-b^2)), \end{aligned} \tag{A9}$$

where we used $\alpha\gamma \le (\alpha^2+\gamma^2)/2 = (1-\beta^2)/2$ and a similar bound over ac. The inequality is saturated if $\alpha = \gamma = \sqrt{(1-\beta^2)/2}$ and $a = c = \sqrt{(1-b^2)/2}$. We parameterize c_0 and c_1 as $c_0 = \cos\theta$ and $c_1 = \sin\theta$, where $\theta \in [0, \pi/2]$. To optimize $f_{\rm av}$, we need to find the maximum of the ternary function

$$\begin{aligned}f_{\rm av}(\beta,b,\theta) = \frac{1}{2} + \frac{\sqrt{3}}{3}(&\cos\theta\sin\theta\beta b \\ &+ \frac{\sqrt{3}}{4}\sin^2\theta(1-\beta^2)(1-b^2)). \end{aligned} \tag{A10}$$

The only stationary points is

$$\frac{\partial f_{\rm av}}{\partial\beta} = \frac{\partial f_{\rm av}}{\partial b} = \frac{\partial f_{\rm av}}{\partial\theta} = 0 \quad \Rightarrow \theta = \frac{\pi}{3}, b = \frac{1}{\sqrt{3}}, \beta = \frac{1}{\sqrt{3}}.$$

However, $f_{\rm av}(\beta = 1/\sqrt{3}, b = 1/\sqrt{3}, \theta = \pi/3) = 2/3$ is not maximal. Indeed, the global maximum is obtained on the boundary (the surface) of the domain $[0,1]\times[0,1]\times[0,\pi/2]$, for $\beta = 1, b = 1, \theta = \pi/4$, with the optimal fidelity score being $f_{\rm max} = f_{\rm av}(\beta = 1, b = 1, \theta = \pi/4) = (3+\sqrt{3})/6$.

Hence, the optimal state is given by $|\Psi_z\rangle = (|\psi^-\rangle + |\psi^+\rangle)/\sqrt{2} = |01\rangle$, corresponding to two anti-aligned spins, and the optimal measurement is given by imposing $|\phi^{\rm sym}\rangle = |\psi^+\rangle$ in $|\eta\rangle$.

c. Measurements with a finite number of outputs

Here we consider the problem of finding an optimal measurement that only requires a finite number of outputs. Suppose we have a *finite* POVM $\{O_{\hat{\mathbf{r}}}\}$ given by $O_{\hat{\mathbf{r}}} = c_{\hat{\mathbf{r}}} U_{\hat{\mathbf{r}}}|\mu\rangle\langle\mu|U_{\hat{\mathbf{r}}}^\dagger$, where $|\mu\rangle$ is a normalized state and $c_{\hat{\mathbf{r}}}$ are positive numbers. Then the average score is given by

$$\begin{aligned}s_{\rm av} &= \sum_{\hat{\mathbf{r}}}\int_{\mathbf{n}} d\mathbf{n} s(\mathbf{n},\hat{\mathbf{r}}) {\rm Tr}\,(O_{\hat{\mathbf{r}}}\Psi_{\mathbf{n}}) \\ &= \sum_{\hat{\mathbf{r}}} {\rm Tr}\left(\int_{\mathbf{n}} d\mathbf{n} s(u_{\hat{\mathbf{r}}}^{-1}u_{\mathbf{n}}) c_{\hat{\mathbf{r}}} U_{\hat{\mathbf{r}}}|\mu\rangle\langle\mu|U_{\hat{\mathbf{r}}}^\dagger U_{\mathbf{n}}\Psi_z U_{\mathbf{n}}^\dagger\right) \\ &= \sum_{\hat{\mathbf{r}}} {\rm Tr}\left(c_{\hat{\mathbf{r}}}|\mu\rangle\langle\mu|\int_{\mathbf{n}} d\mathbf{n} s(\mathbf{n},+\mathbf{z}) U_{\mathbf{n}}\Psi_z U_{\mathbf{n}}^\dagger\right) \\ &= \sum_{\hat{\mathbf{r}}} c_{\hat{\mathbf{r}}} {\rm Tr}\,(|\mu\rangle\langle\mu|F) \\ &= 4{\rm Tr}\,(|\mu\rangle\langle\mu|F)\,. \end{aligned} \tag{A11}$$

The last equality follows from the completeness condition $\sum_{\hat{\mathbf{r}}} O_{\hat{\mathbf{r}}} = \mathbb{1}$, which gives $\sum_{\hat{\mathbf{r}}} c_{\hat{\mathbf{r}}} = 4$ by our tracing both sides. Taking $|\mu\rangle = 1/2|\psi^-\rangle + \sqrt{3}/2|\phi^{\rm sym}\rangle$, we reach the same result as Eq. (A1). Thus, the optimization of $|\phi^{\rm sym}\rangle$ and the initial state gives the same results as the covariant-POVM case. We just need to find a set of $\{U_{\hat{\mathbf{r}}}\}$ and $\{c_{\hat{\mathbf{r}}}\}$ to generate a *finite* POVM from $|\mu\rangle\langle\mu|$.

In the case of $|\phi^{\rm sym}\rangle = |\psi^+\rangle$, i.e., $|\mu\rangle = 1/2|\psi^-\rangle + \sqrt{3}/2|\psi^+\rangle$, the POVM can be taken to be the elegant joint

measurement $\Pi^0_{\hat{\mathbf{n}}_i} = |\Phi^0_{\hat{\mathbf{n}}_i}\rangle\langle\Phi^0_{\hat{\mathbf{n}}_i}|$, where

$$|\Phi^0_{\hat{\mathbf{n}}_i}\rangle = \frac{1}{2}|\psi^-_{\hat{\mathbf{n}}_i}\rangle + \frac{\sqrt{3}}{2}|\psi^+_{\hat{\mathbf{n}}_i}\rangle, \quad i = 1,2,3,4, \tag{A12}$$

and $\hat{\mathbf{n}}_i$ points at the four extremities of a tetrahedron.

2. Direction guessing assisted by abstention

Let $\bar{\Pi}_{\text{abst}} = \mathbb{1} - \Pi_{\text{abst}} = \bar{\lambda}_0 \mathbb{1}_{\mathcal{H}_0} + \bar{\lambda}_1 \mathbb{1}_{\mathcal{H}_1}$, where $\bar{\lambda}_j = 1 - \lambda_j$. Introducing the new POVM elements

$$\tilde{\Pi}_{\hat{\mathbf{n}}} = \bar{\Pi}^{-1/2}_{\text{abst}} \Pi_{\hat{\mathbf{n}}} \bar{\Pi}^{-1/2}_{\text{abst}} \tag{A13}$$

and the new family of states

$$|\tilde{\Psi}_{\mathbf{n}}\rangle = \left(\frac{\bar{\Pi}_{\text{abst}}}{\bar{Q}}\right)^{1/2} |\Psi_{\mathbf{n}}\rangle, \tag{A14}$$

we can rewrite the average score given by Eq. (10) as

$$\begin{aligned} s_{\text{av}} &= \int d\mathbf{n} d\hat{\mathbf{n}} s(\mathbf{n},\hat{\mathbf{n}}) \text{Tr}\left(\tilde{\Pi}_{\hat{\mathbf{n}}} \tilde{\Psi}_{\mathbf{n}}\right) \\ &= \int d\mathbf{n} d\hat{\mathbf{n}} s(u^{-1}_{\hat{\mathbf{n}}} u_{\mathbf{n}}) \text{Tr}\left(U_{\hat{\mathbf{n}}} \tilde{\Pi}_z U^\dagger_{\hat{\mathbf{n}}} \cdot U_{\mathbf{n}} \tilde{\Psi}_z U^\dagger_{\mathbf{n}}\right) \\ &= \int d\mathbf{n} s(\mathbf{n},+\mathbf{z}) \text{Tr}\left(\tilde{\Pi}_z U_{\mathbf{n}} \tilde{\Psi}_z U^\dagger_{\mathbf{n}}\right), \end{aligned} \tag{A15}$$

implying that we are back at the standard estimation problem with POVM seed $\tilde{\Pi}_z$ and initial state $|\tilde{\Psi}_z\rangle = \tilde{c}_0|\psi^-\rangle + \tilde{c}_1|\psi^{\text{sym}}\rangle$, where

$$\tilde{c}_i = \sqrt{\frac{\bar{\lambda}_i}{\bar{Q}}} c_i. \tag{A16}$$

a. Maximum likelihood score

Similarly to the standard estimation problem, it is best to take $\tilde{\Pi}_z = |\eta\rangle\langle\eta|$ with $|\eta\rangle = |\psi^-\rangle + \sqrt{3}|\psi^{\text{sym}}\rangle$, and the optimization problem becomes

$$\delta_{\max} = \max_{\substack{|\tilde{c}_j| \le |c_j|/\sqrt{\bar{Q}} \\ |\tilde{c}_0|^2 + |\tilde{c}_1|^2 = 1}} |\tilde{c}_0 + \sqrt{3}\tilde{c}_1|^2. \tag{A17}$$

Hence, Alice cannot increase the maximum score $\delta_{\max} = 4$ whatever the initial state and the abstention rate. However, with $\bar{Q} \le \min(4c_0^2, \frac{4}{3}c_1^2)$, Alice can always reach $\delta_{\max}$ when she tunes $\bar{\lambda}_0$ and $\bar{\lambda}_1$ such that $\tilde{c}_0 = 1/2$ and $\tilde{c}_1 = \sqrt{3}/2$. This is obtained for

$$\bar{\lambda}_0 = \frac{\bar{Q}}{4c_0^2}, \quad \bar{\lambda}_1 = \frac{3\bar{Q}}{4c_1^2}. \tag{A18}$$

Hence, Alice can reach $\delta_{\max}$ if she is allowed to not answer sufficiently often, under the unique condition that $c_0, c_1 \neq 0$.

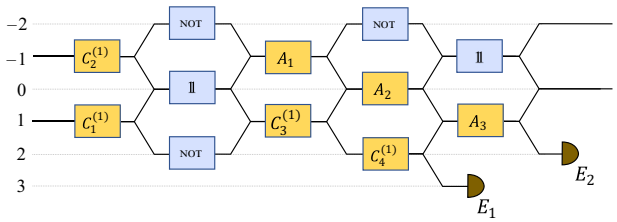

FIG. 4. Simplification of the combination of module 1 and module 2 of the measurement device under the condition of Eq. (B1).

b. Fidelity score

It is best to take $|\tilde{\Psi}_z\rangle = 1/\sqrt{2}|\psi^-\rangle + 1/\sqrt{2}|\psi^+\rangle$ and $\tilde{\Pi}_z = |\eta\rangle\langle\eta|$ with $|\eta\rangle = |\psi^-\rangle + \sqrt{3}|\psi^+\rangle$. With $\bar{Q} \le \min(2c_0^2, 2c_1^2)$, Alice can always reach $f_{\max} = (3+\sqrt{3})/6$ when she tunes $\bar{\lambda}_0$ and $\bar{\lambda}_1$ such that $\tilde{c}_0 = \tilde{c}_1 = 1/\sqrt{2}$. This is obtained for

$$\bar{\lambda}_i = \frac{\bar{Q}}{2c_i^2}, \quad i = 1,2, \tag{A19}$$

under the unique condition that $c_0, c_1 \neq 0$.

c. Optimal measurements with a finite number of outputs

Using Eqs. (A12) and (A13), one can show that in the case of $|\phi^{\text{sym}}\rangle = |\psi^+\rangle$, the optimal POVM elements (in addition to Π_{abst}) can be taken to be four rank-1 elements $\Pi_{\hat{\mathbf{n}}_i} = |\Phi_{\hat{\mathbf{n}}_i}\rangle\langle\Phi_{\hat{\mathbf{n}}_i}|$, where

$$|\Phi_{\hat{\mathbf{n}}_i}\rangle = \frac{\sqrt{\bar{\lambda}_0}}{2}|\psi^-_{\hat{\mathbf{n}}_i}\rangle + \frac{\sqrt{3\bar{\lambda}_1}}{2}|\psi^+_{\hat{\mathbf{n}}_i}\rangle, \quad i = 1,2,3,4. \tag{A20}$$

APPENDIX B: SIMPLIFICATION OF THE MEASUREMENT DEVICE FOR THE OPTIMAL ABSTENTION POVM

In this appendix, we explain how we simplify our universal measurement device to realize the optimal abstention POVM given in Eq. (12) [also in Eq. (A20)] with $\bar{\lambda}_1 = 1$. Figure 1 shows a quantum-walk construction for implementing an arbitrary two-qubit POVM $\{E_1, E_2, \ldots, E_n\}$, where $E_i = a_i|\psi_i\rangle\langle\psi_i|$. According to the algorithm presented in Sec. II, the first three steps in module 1 can be seen as a projection on $|\psi_1\rangle$ (because $K_1 = \mathbb{1}$ and $b_1 = 1$), where the component of $|\psi_1\rangle$ is completely transformed into $|1\rangle$ and then enters path 2 after the third step. Using this projection, we decompose $|\psi_2\rangle$ as $|\psi_2\rangle = p|\psi_1\rangle + q|\psi_1^\perp\rangle$. Then the combination of module 1 and module 2 can be simplified into the structure shown in Fig. 4 under

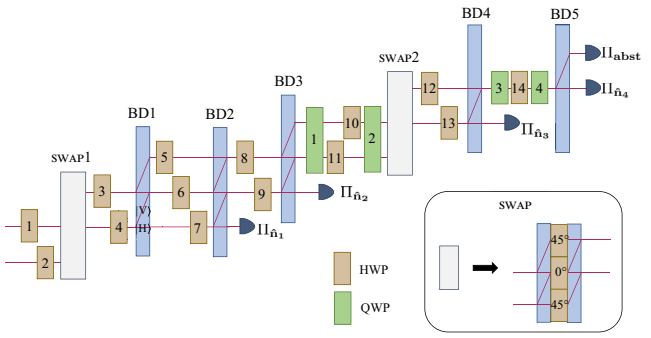

FIG. 5. Realization of the two-qubit abstention POVMs with $\bar{\lambda}_1 = 1$ using nine-step photonic quantum walks. H, horizontal polarization; V, vertical polarization.

the condition

$$a_2|q|^2 + \frac{a_2|p|^2}{1-a_1} = 1. \tag{B1}$$

Here, coin operators $C_1^{(1)}$, $C_2^{(1)}$ $C_3^{(1)}$, and $C_4^{(1)}$ are still determined by the algorithm in Sec. II. A_1 and A_2 are chosen such that

$$\begin{pmatrix} 1 & 0 \\ 0 & 0 \\ 0 & 0 \\ 0 & 1 \end{pmatrix} A_2 \begin{pmatrix} 0 & 0 & 1 & 0 \\ 0 & 1 & 0 & 0 \end{pmatrix} \begin{pmatrix} C_3^{(1)} & 0 \\ 0 & A_1 \end{pmatrix}$$

$$\begin{pmatrix} 0 & 0 & 1 & 0 \\ 1 & 0 & 0 & 0 \\ 0 & 0 & 0 & 1 \\ 0 & 1 & 0 & 0 \end{pmatrix} \begin{pmatrix} C_1^{(1)} & 0 \\ 0 & C_2^{(1)} \end{pmatrix} |\psi_1^{\perp}\rangle = \begin{pmatrix} 1 \\ 0 \\ 0 \\ 0 \end{pmatrix}, \tag{B2}$$

implying that the component of $|\psi_1^{\perp}\rangle$ is transformed into $|1\rangle$ after the fourth step. The coin operator A_3 is set as

$$A_3 = \begin{pmatrix} \sqrt{a_2}q & \frac{\sqrt{a_2}p^*}{\sqrt{1-a_1}} \\ \frac{\sqrt{a_2}p}{\sqrt{1-a_1}} & -\sqrt{a_2}q^* \end{pmatrix}. \tag{B3}$$

Thus, the amplitude entering path 2 after the fifth step reads

$$\begin{aligned} &(\sqrt{a_2}q\langle\psi^{\perp}| + \frac{\sqrt{a_2}p}{\sqrt{1-a_1}}\sqrt{1-a_1}\langle\psi_1|)|\varphi\rangle \\ &= \sqrt{a_2}(q\langle\psi_1^{\perp}| + p\langle\psi_1|)|\varphi\rangle \\ &= \sqrt{a_2}\langle\psi_2|\varphi\rangle, \end{aligned} \tag{B4}$$

demonstrating the implementation of E_2.

Considering the optimal abstention POVM $\{\Pi_{\hat{\mathbf{n}}}\} \cup \{\Pi_{\text{abst}}\}$, if $\bar{\lambda}_1 = 1$, the quantum-walk construction can be simplified because the condition in Eq. (B1) is satisfied. Additionally, the fourth step in module 3 and module 4 can be removed because $C_4^{(3)} = C_4^{(4)} = \mathbb{1}$. Moreover, noting that $C_1^{(4)} = C_2^{(4)} = \text{NOT}$, we find that the first two steps in module 4 can be removed by replacing the coin operator $\mathbb{1}$ in the third step of module 3 with a NOT gate. Finally, the optimal abstention POVM with $\bar{\lambda}_1 = 1$ can be realized with a nine-step quantum walk, shown in Fig. 2 (also in Fig. 5).

APPENDIX C: EXPERIMENTAL STATE PREPARATION

In this appendix, we give experimental details about how we prepare the encoding state using the state-preparation module shown in Fig. 2. A light pulse from a mode-locked Ti:sapphire laser at 780 nm passes through a frequency doubler, and then pumps a 2-mm-long β-barium borate crystal. After the type-II phase-matched spontaneous-parametric-down-conversion process, a pair of photons at 780 nm is created. The two photons are coupled to two single-mode fibers. One photon acts as a trigger, while the other is used as a single-photon source and is initialized with horizontal polarization by a PBS. After it has passed through a HWP and a QWP, any polarization state can be generated. BD0 translates the polarization state into the path DOF, and thus the walker qubit is prepared. The following combinations of the five wave plates transform the Bloch vectors $\{+\mathbf{z}, -\mathbf{z}\}$ of the polarization state at positions 1 and -1 into the desired $\{\mathbf{m_1}, \mathbf{m_2}\}$ to prepare the coin qubit.

Note that for the maximum likelihood score, only the ability to perform perfect guesses matters. Hence, we consider only sending each of the four tetrahedral directions $\{\hat{\mathbf{n}}_1, \hat{\mathbf{n}}_2, \hat{\mathbf{n}}_3, \hat{\mathbf{n}}_4\}$ to the measurement device [53]. For the fidelity score, we restrict the input states to be one of the six directions $\{\pm\mathbf{x}, \pm\mathbf{y}, \pm\mathbf{z}\}$, which is an alternative to the direction randomly selected from the unit sphere. This way to select the input direction of the state corresponds to the same operator $F_f\,(|\psi^{\text{sym}}\rangle = |\psi^+\rangle)$:

$$\begin{aligned} F_f\,(|\psi^{\text{sym}}\rangle{=}|\psi^+\rangle) &= \sum_{\mathbf{n}\in\{\pm\mathbf{x},\pm\mathbf{y},\pm\mathbf{z}\}} \frac{1}{6}\cdot f\,(\mathbf{n}) U_{\mathbf{n}} \Psi_z U_{\mathbf{n}}^{\dagger} \\ &= \frac{|c_0|^2}{2}\mathbb{1}_{\mathcal{H}_0} + \frac{|c_1|^2}{6}\mathbb{1}_{\mathcal{H}_1} + \frac{c_0 c_1^*}{6}(|\psi^-\rangle\langle\psi^+| + \text{c.c.}), \end{aligned} \tag{C1}$$

giving the same result as Eq. (A7).

TABLE II. Rotation angles (degrees) of the wave plates in Fig. 5 that are constant.

HWP1	HWP2	HWP3	HWP5	HWP8	HWP10	HWP12	QWP1	QWP2	QWP3	QWP4
0	45	67.5	45	0	45	135	0	0	0	0

TABLE III. Specific c_0 of the input state we choose for the maximum likelihood score and the corresponding optimized $\bar{\lambda}_0$ and the rotation angles (degrees) of the wave plates dependent on $\bar{\lambda}_0$.

c_0	$\bar{\lambda}_0$	HWP4	HWP6	HWP7	HWP9	HWP11	HWP13	HWP14
0.5	1	37.5	−17.6322	0	0	90	67.5	135
0.6	0.5926	34.4812	−14.9358	9.3055	−9.8396	76.5853	63.7945	154.832
0.7	0.3469	31.8908	−12.2404	11.9161	−13.107	72.5750	60.2494	161.9564
0.8	0.1875	29.5181	−9.4659	13.3941	−15.1616	70.2017	56.7066	167.1705
0.9	0.0782	27.0854	−6.3509	14.3445	−16.5887	68.6211	52.8111	81.8811

APPENDIX D: ROTATION ANGLES OF THE WAVE PLATES IN THE MEASUREMENT DEVICE

In this appendix, we present the specific rotation angles of the wave plates in the measurement module in Fig. 2 (also in Fig. 5). In our experiment, we choose the tetrahedral directions as

$$\begin{aligned}
|\hat{\mathbf{n}}_1\rangle&=|0\rangle, \qquad |\hat{\mathbf{n}}_2\rangle=\frac{i}{\sqrt{3}}(|0\rangle+\sqrt{2}|1\rangle),\\
|\hat{\mathbf{n}}_3\rangle&=\frac{i}{\sqrt{3}}(|0\rangle+e^{\frac{2\pi}{3}i}\sqrt{2}|1\rangle),\\
|\hat{\mathbf{n}}_4\rangle&=\frac{i}{\sqrt{3}}(-|0\rangle+e^{\frac{\pi}{3}i}\sqrt{2}|1\rangle).
\end{aligned} \tag{D1}$$

Because we let $\bar{\lambda}_1 = 1$, for the maximum likelihood score, the optimization condition [Eq. (A18)] is achievable when $1/2 \le c_0 < 1$, and for the fidelity score, the optimization condition [Eq. (A19)] is achievable when $\sqrt{2}/2 \le c_0 < 1$. WE choose the coefficient c_0 of the input state in the experiment, and the corresponding rotation angles of the wave plates are specified in Tables II–IV. Here some rotation angles are constant whatever $\bar{\lambda}_0$ is taken, and some are dependent on $\bar{\lambda}_0$.

APPENDIX E: ERROR ANALYSIS OF THE EXPERIMENTAL SCORE

In Fig. 3, the experimental deviation of the average score $|\Delta s| = |s_{\text{expt}} - s_{\text{ideal}}|$ increases with increase of the abstention rate Q. We show here that this comes from the amplification of the experimental error by the term $1/(1-Q)$ in Eq. (10).

As mentioned in Appendix C, for the maximum likelihood score we input each of the four directions $\{\hat{\mathbf{n}}_1, \hat{\mathbf{n}}_2, \hat{\mathbf{n}}_3, \hat{\mathbf{n}}_4\}$ into the measurement device, and for the fidelity score, we input each of the six directions $\{\pm\mathbf{x}, \pm\mathbf{y}, \pm\mathbf{z}\}$. Therefore, the ideal score is given by

$$s_{\text{ideal}} = \frac{1}{1-Q_{\text{ideal}}}\frac{1}{k}\sum_{j=1}^{k}\sum_{i=1}^{4} s(\mathbf{n}_j, \hat{\mathbf{n}}_i)\text{Tr}\left(\Pi_{\hat{\mathbf{n}}_i}\Psi_{\mathbf{n}_j}\right), \tag{E1}$$

where $Q_{\text{ideal}} = 1/k\sum_{j=1}^{k}\text{Tr}\left(\Pi_{\text{abst}}\Psi_{\mathbf{n}_j}\right)$ and $k = 4$ ($k = 6$) for the maximum likelihood (fidelity) score.

In our experimental setup, we prepare $N_{\mathbf{n}_j} = N_0 = 20\,000$ photons for each input direction $\mathbf{n}_j$, and we obtain either a guess $\hat{\mathbf{n}}_i$ or an abstention output. Let $\{\{N_{\mathbf{n}_j,\hat{\mathbf{n}}_i}\}, N_{\mathbf{n}_j,\text{abst}}\}$ be the respective number of times these events happened ($N_{\mathbf{n}_j} = \sum_i N_{\mathbf{n}_j,\hat{\mathbf{n}}_i} + N_{\mathbf{n}_j,\text{abst}}$). The experimental score is given by

$$\begin{aligned}
s_{\text{expt.}} &= \frac{\sum_{j=1}^{k}\sum_{i=1}^{4} s(\mathbf{n}_j, \hat{\mathbf{n}}_i)N_{\mathbf{n}_j,\hat{\mathbf{n}}_i}}{\sum_{j=1}^{k}\sum_{i=1}^{4} N_{\mathbf{n}_j,\hat{\mathbf{n}}_i}}\\
&= \frac{\sum_{j=1}^{k}\sum_{i=1}^{4} s(\mathbf{n}_j, \hat{\mathbf{n}}_i)N_{\mathbf{n}_j,\hat{\mathbf{n}}_i}}{\sum_{j=1}^{k}(N_0 - N_{\mathbf{n}_j,\text{abst}})}\\
&= \frac{1}{1-\frac{1}{k}\sum_{j=1}^{k}\frac{N_{\mathbf{n}_j,\text{abst}}}{N_0}}\frac{1}{k}\sum_{j=1}^{k}\sum_{i=1}^{4} s(\mathbf{n}_j, \hat{\mathbf{n}}_i)\frac{N_{\mathbf{n}_j,\hat{\mathbf{n}}_i}}{N_0}\\
&= \frac{1}{1-Q_{\text{expt.}}}\frac{1}{k}\sum_{j=1}^{k}\sum_{i=1}^{4} s(\mathbf{n}_j, \hat{\mathbf{n}}_i)\hat{p}(\mathbf{n}_j, \hat{\mathbf{n}}_i),
\end{aligned} \tag{E2}$$

where $\hat{p}(\mathbf{n}_j, \hat{\mathbf{n}}_i) = N_{\mathbf{n}_j,\hat{\mathbf{n}}_i}/N_0$ is the frequency of guess $\hat{\mathbf{n}}_i$ when the input direction is $\mathbf{n}_j$, and $Q_{\text{expt.}} = 1/k\sum_{j=1}^{k} N_{\mathbf{n}_j,\text{abst}}/N_0 = 1/k\sum_{j=1}^{k}\hat{p}(\mathbf{n}_{j,\text{abst}})$ is the experimental

TABLE IV. Specific c_0 of the input state we choose for the fidelity score and the corresponding optimized $\bar{\lambda}_0$ and the rotation angles (degrees) of the wave plates dependent on $\bar{\lambda}_0$.

c_0	$\bar{\lambda}_0$	HWP4	HWP6	HWP7	HWP9	HWP11	HWP13	HWP14
0.7071	1	37.5	−17.6322	0	0	90	67.5	135
0.7571	0.7446	35.7409	−16.1181	7.3188	−7.5701	79.5303	65.3951	150.1793
0.8071	0.5351	33.9481	−14.4101	9.9664	−10.6312	75.5878	63.0929	156.4935
0.8571	0.3612	32.0684	−12.4365	11.7771	−12.9225	72.7939	60.5034	161.5285
0.9071	0.2153	29.9985	−10.0501	13.1451	−14.8025	70.6083	57.4457	166.1771

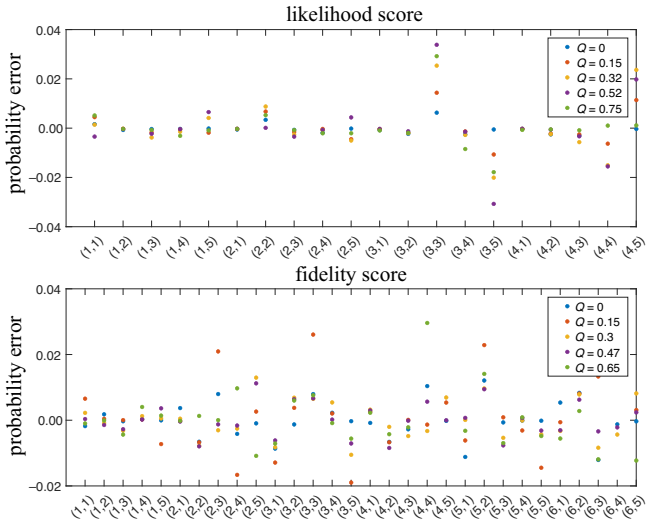

FIG. 6. Experimental errors of the probabilities $\mathrm{Tr}\left(\Pi_i \Psi_{\mathbf{n}_j}\right)$, where $\Pi_i = \Pi_{\hat{\mathbf{n}}_i}$ for $i = 1, \ldots, 4$ and $\Pi_5 = \Pi_{\mathrm{abst}}$. The coordinates of the x axis represent all the combinations $(\Psi_{\mathbf{n}_j}, \Pi_i)$. Experimental errors for different abstention rates are marked in different colors, which shows approximate independence of Q.

abstention rate, where $\hat{p}(\mathbf{n}_{j,\mathrm{abst}})$ is the abstention frequency for $\mathbf{n}_j$.

To analyze the deviation, we introduce $r_{\mathrm{ideal}} = 1/k \sum_{j=1}^{k} \sum_{i=1}^{4} s(\mathbf{n}_j, \hat{\mathbf{n}}_i) \mathrm{Tr}\left(\Pi_{\hat{\mathbf{n}}_i} \Psi_{\mathbf{n}_j}\right)$ and $r_{\mathrm{expt.}} = 1/k \sum_{j=1}^{k} \sum_{i=1}^{4} s(\mathbf{n}_j, \hat{\mathbf{n}}_i) \hat{p}(\mathbf{n}_j, \hat{\mathbf{n}}_i)$. Then we have

$$\begin{aligned}
\Delta s &= s_{\mathrm{expt.}} - s_{\mathrm{ideal}} \\
&= \frac{1}{1 - Q_{\mathrm{expt.}}} r_{\mathrm{expt.}} - \frac{1}{1 - Q_{\mathrm{ideal}}} r_{\mathrm{ideal}} \\
&= \frac{1}{1 - Q_{\mathrm{expt.}}} (r_{\mathrm{expt.}} - r_{\mathrm{ideal}}) \\
&\quad + \frac{Q_{\mathrm{expt.}} - Q_{\mathrm{ideal}}}{(1 - Q_{\mathrm{expt.}})(1 - Q_{\mathrm{ideal}})} r_{\mathrm{ideal}} \\
&= \frac{1}{1 - Q_{\mathrm{expt.}}} (\Delta r + s_{\mathrm{ideal}} \Delta Q), \qquad \text{(E3)}
\end{aligned}$$

where s_{ideal} is independent of Q, $\Delta r = r_{\mathrm{expt.}} - r_{\mathrm{ideal}} = 1/k \sum_{j=1}^{k} \sum_{i=1}^{4} s(\mathbf{n}_j, \hat{\mathbf{n}}_i)[\hat{p}(\mathbf{n}_j, \hat{\mathbf{n}}_i) - \mathrm{Tr}\left(\Pi_{\hat{\mathbf{n}}_i} \Psi_{\mathbf{n}_j}\right)]$, and $\Delta Q = Q_{\mathrm{expt.}} - Q_{\mathrm{ideal}} = 1/k \sum_{j=1}^{k} [\hat{p}(\mathbf{n}_{j,\mathrm{abst}}) - \mathrm{Tr}\left(\Pi_{\mathrm{abst}} \Psi_{\mathbf{n}_j}\right)]$. Δr and ΔQ depend only on the experimental error of the probabilities $\mathrm{Tr}\left(\Pi_{\hat{\mathbf{n}}_i} \Psi_{\mathbf{n}_j}\right)$ and $\mathrm{Tr}\left(\Pi_{\mathrm{abst}} \Psi_{\mathbf{n}_j}\right)$, which come from the imperfection of the experimental apparatus and are to a good approximation independent of Q, as shown in Fig. 6. However, the term $1/(1 - Q_{\mathrm{expt.}})$ amplifies this experimental error, and thus $|\Delta s|$ tends increase with increase of $Q_{\mathrm{expt.}}$.

[1] C. W. Helstrom, *Quantum Detection and Estimation Theory* (Academic Press, New York, 1976).

[2] M. A. Nielsen and I. L. Chuang, *Quantum Computation and Quantum Information* (Cambridge University Press, Cambridge, UK, 2000).

[3] N. Gisin, G. Ribordy, W. Tittel, and H. Zbinden, Quantum cryptography, Rev. Mod. Phys. **74**, 145 (2002).

[4] I. Šupić and J. Bowles, Self-testing of quantum systems: A review, Quantum **4**, 337 (2020).

[5] M. O. Renou, J. Kaniewski, and N. Brunner, Self-testing entangled measurements in quantum networks, Phys. Rev. Lett. **121**, 250507 (2018).

[6] J.-D. Bancal, N. Sangouard, and P. Sekatski, Noise-resistant device-independent certification of bell state measurements, Phys. Rev. Lett. **121**, 250506 (2018).

[7] I. Šupić, J. Bowles, M.-O. Renou, A. Acín, and M. J. Hoban, Quantum networks self-test all entangled states, Nat. Phys. **19**, 670 (2023).

[8] V. Giovannetti, S. Lloyd, and L. Maccone, Advances in quantum metrology, Nat. Photonics **5**, 222 (2011).

[9] S. Massar, Collective versus local measurements on two parallel or antiparallel spins, Phys. Rev. A **62**, 040101(R) (2000).

[10] G. Zauner, Quantum designs: Foundations of a noncommutative design theory, Int. J. Quantum Inf. **9**, 445 (2011).

[11] N. Li, C. Ferrie, J. A. Gross, A. Kalev, and C. M. Caves, Fisher-symmetric informationally complete measurements for pure states, Phys. Rev. Lett. **116**, 180402 (2016).

[12] H. Zhu and M. Hayashi, Universally Fisher-symmetric informationally complete measurements, Phys. Rev. Lett. **120**, 030404 (2018).

[13] E. Bagan, M. A. Ballester, R. D. Gill, R. Muñoz-Tapia, and O. Romero-Isart, Separable measurement estimation of density matrices and its fidelity gap with collective protocols, Phys. Rev. Lett. **97**, 130501 (2006).

[14] A. Peres and W. K. Wootters, Optimal detection of quantum information, Phys. Rev. Lett. **66**, 1119 (1991).

[15] S. Massar and S. Popescu, Optimal extraction of information from finite quantum ensembles, Phys. Rev. Lett. **74**, 1259 (1995).

[16] N. Gisin and S. Popescu, Spin flips and quantum information for antiparallel spins, Phys. Rev. Lett. **83**, 432 (1999).

[17] M. D. Vidrighin, G. Donati, M. G. Genoni, X.-M. Jin, W. S. Kolthammer, M. S. Kim, A. Datta, M. Barbieri, and I. A. Walmsley, Joint estimation of phase and phase diffusion for quantum metrology, Nat. Commun. **5**, 3532 (2014).

[18] E. Roccia, I. Gianani, L. Mancino, M. Sbroscia, F. Somma, M. G. Genoni, and M. Barbieri, Entangling measurements for multiparameter estimation with two qubits, Quantum Sci. Technol. **3**, 01LT01 (2018).

[19] N. Linden, S. Massar, and S. Popescu, Purifying noisy entanglement requires collective measurements, Phys. Rev. Lett. **81**, 3279 (1998).

[20] M. Fanizza, M. Rosati, M. Skotiniotis, J. Calsamiglia, and V. Giovannetti, Beyond the swap test: optimal estimation of quantum state overlap, Phys. Rev. Lett. **124**, 060503 (2020).

[21] G. Sentís, E. Bagan, J. Calsamiglia, G. Chiribella, and R. Muñoz-Tapia, Quantum change point, Phys. Rev. Lett. **117**, 150502 (2016).

[22] M. Perarnau-Llobet, E. Bäumer, K. V. Hovhannisyan, M. Huber, and A. Acin, No-go theorem for the characterization of work fluctuations in coherent quantum systems, Phys. Rev. Lett. **118**, 070601 (2017).

[23] K.-D. Wu, E. Bäumer, J.-F. Tang, K. V. Hovhannisyan, M. Perarnau-Llobet, G.-Y. Xiang, C.-F. Li, and G.-C. Guo, Minimizing backaction through entangled measurements, Phys. Rev. Lett. **125**, 210401 (2020).

[24] J. M. Renes, R. Blume-Kohout, A. J. Scott, and C. M. Caves, Symmetric informationally complete quantum measurements, J. Math. Phys. **45**, 2171 (2004).

[25] J. A. Bergou, U. Futschik, and E. Feldman, Optimal unambiguous discrimination of pure quantum states, Phys. Rev. Lett. **108**, 250502 (2012).

[26] E. Bagan, R. Muñoz-Tapia, G. A. Olivares-Rentería, and J. A. Bergou, Optimal discrimination of quantum states with a fixed rate of inconclusive outcomes, Phys. Rev. A **86**, 040303(R) (2012).

[27] B. Gendra, E. Ronco-Bonvehi, J. Calsamiglia, R. Muñoz-Tapia, and E. Bagan, Quantum metrology assisted by abstention, Phys. Rev. Lett. **110**, 100501 (2013).

[28] B. Gendra, E. Ronco-Bonvehi, J. Calsamiglia, R. Muñoz-Tapia, and E. Bagan, Optimal parameter estimation with a fixed rate of abstention, Phys. Rev. A **88**, 012128 (2013).

[29] I. Ivanovic, How to differentiate between non-orthogonal states, Phys. Lett. A **123**, 257 (1987), ISSN issn0375-9601.

[30] M. Mohseni, A. M. Steinberg, and J. A. Bergou, Optical realization of optimal unambiguous discrimination for pure and mixed quantum states, Phys. Rev. Lett. **93**, 200403 (2004).

[31] Z. Hou, J.-F. Tang, J. Shang, H. Zhu, J. Li, Y. Yuan, K.-D. Wu, G.-Y. Xiang, C.-F. Li, and G.-C. Guo, Deterministic realization of collective measurements via photonic quantum walks, Nat. Commun. **9**, 1414 (2018).

[32] Y. Yuan, Z. Hou, J.-F. Tang, A. Streltsov, G.-Y. Xiang, C.-F. Li, and G.-C. Guo, Direct estimation of quantum coherence by collective measurements, Npj Quantum Inf. **6**, 46 (2020).

[33] J.-F. Tang, Z. Hou, J. Shang, H. Zhu, G.-Y. Xiang, C.-F. Li, and G.-C. Guo, Experimental optimal orienteering via parallel and antiparallel spins, Phys. Rev. Lett. **124**, 060502 (2020).

[34] L. O. Conlon, T. Vogl, C. D. Marciniak, I. Pogorelov, S. K. Yung, F. Eilenberger, D. W. Berry, F. S. Santana, R. Blatt, T. Monz, Ping Koy Lam, and Syed M. Assad, Approaching optimal entangling collective measurements on quantum computing platforms, Nat. Phys. **19**, 351 (2023).

[35] P. Kurzyński and A. Wójcik, Quantum walk as a generalized measuring sevice, Phys. Rev. Lett. **110**, 200404 (2013).

[36] E. Bagan, M. Baig, A. Brey, R. Muñoz-Tapia, and R. Tarrach, Optimal encoding and decoding of a spin direction, Phys. Rev. A **63**, 052309 (2001).

[37] A. Peres and P. F. Scudo, Transmission of a Cartesian frame by a quantum system, Phys. Rev. Lett. **87**, 167901 (2001).

[38] A. Peres and P. Scudo, Covariant quantum measurements may not be optimal, J. Mod. Opt. **49**, 1235 (2002).

[39] E. Bagan, M. Baig, and R. Muñoz-Tapia, Quantum reverse engineering and reference-frame alignment without nonlocal correlations, Phys. Rev. A **70**, 030301(R) (2004).

[40] G. Chiribella, G. M. D'Ariano, P. Perinotti, and M. F. Sacchi, Efficient use of quantum resources for the transmission of a reference frame, Phys. Rev. Lett. **93**, 180503 (2004).

[41] M. Fiorentino and F. N. C. Wong, Deterministic controlled-NOT gate for single-photon two-qubit quantum logic, Phys. Rev. Lett. **93**, 070502 (2004).

[42] J. T. Barreiro, T.-C. Wei, and P. G. Kwiat, Beating the channel capacity limit for linear photonic superdense coding, Nat. Phys. **4**, 282 (2008).

[43] B. P. Lanyon, M. Barbieri, M. P. Almeida, T. Jennewein, T. C. Ralph, K. J. Resch, G. J. Pryde, J. L. O'brien, A. Gilchrist, and A. G. White, Simplifying quantum logic using higher-dimensional Hilbert spaces, Nat. Phys. **5**, 134 (2009).

[44] G. Rubino, L. A. Rozema, A. Feix, M. Araújo, J. M. Zeuner, L. M. Procopio, Č. Brukner, and P. Walther, Experimental verification of an indefinite causal order, Sci. Adv. **3**, e1602589 (2017).

[45] C. Vitelli, N. Spagnolo, L. Aparo, F. Sciarrino, E. Santamato, and L. Marrucci, Joining the quantum state of two photons into one, Nat. Photonics **7**, 521 (2013).

[46] Z. Li, H. Zhang, and H. Zhu, Implementation of generalized measurements on a qudit via quantum walks, Phys. Rev. A **99**, 062342 (2019).

[47] Z. Bian, J. Li, H. Qin, X. Zhan, R. Zhang, B. C. Sanders, and P. Xue, Realization of single-qubit positive-operator-valued measurement via a one-dimensional photonic quantum walk, Phys. Rev. Lett. **114**, 203602 (2015).

[48] Y.-Y. Zhao, N.-K. Yu, P. Kurzyński, G.-Y. Xiang, C.-F. Li, and G.-C. Guo, Experimental realization of generalized qubit measurements based on quantum walks, Phys. Rev. A **91**, 042101 (2015).

[49] The maximum likelihood score should be understood asymptotically. $\delta(\mathbf{n},\hat{\mathbf{n}}) = p(\hat{\mathbf{n}} \in d\mathcal{A})/|d\mathcal{A}|$, where $d\mathcal{A}$ is an infinitesimally small subset $d\mathcal{A} \subset \mathrm{SU}(2)$ containing $\mathbf{n}$ and $|d\mathcal{A}|$ is its area. For instance, if SU(2) is divided into four parts of equal area and Alice is exactly able to guess in which of these four parts $\mathbf{n}$ is, then $\delta(\mathbf{n},\hat{\mathbf{n}}) = 4$.

[50] J. Fiurášek, Maximum-likelihood estimation of quantum measurement, Phys. Rev. A **64**, 024102 (2001).

[51] J. Wang, F. Sciarrino, A. Laing, and M. G. Thompson, Integrated photonic quantum technologies, Nat. Photonics **14**, 273 (2020).

[52] G. Chiribella, Group theoretic structures in the estimation of an unknown unitary transformation, J. Phys. Conf. Ser. **284**, 012001 (2011).

[53] A rigorous justification of our experimental procedure is as follows. At each trial, Alice chooses a redefinition of direction $\mathbf{z}$ and sends direction $\{\hat{\mathbf{n}}_1,\hat{\mathbf{n}}_2,\hat{\mathbf{n}}_3,\hat{\mathbf{n}}_4\}$ to the referee in charge of computing $\delta(\mathbf{n},\hat{\mathbf{n}})$. If $\mathbf{n} \notin \{\hat{\mathbf{n}}_1,\hat{\mathbf{n}}_2,\hat{\mathbf{n}}_3,\hat{\mathbf{n}}_4\}$, the referee attributes a score of 0 to Alice without even sending the state $|\psi_{\mathbf{n}}\rangle$ to her. Otherwise, the referee sends $|\psi_{\mathbf{n}}\rangle$ and checks if Alice made the correct guess. This procedure can be understood asymptotically, given a discretization of the sphere into small subsets $d\mathcal{A}$.